THE JOURNAL OF PHYSICAL CHEMISTRY B

Article

pubs.acs.org/JPCB

How Large Should the QM Region Be in QM/MM Calculations? The Case of Catechol *O*-Methyltransferase

Heather J. Kulik,[†,‡,∥] Jianyu Zhang,[§] Judith P. Klinman,[§] and Todd J. Martínez*[,†,‡]

[†]Department of Chemistry and PULSE Institute, Stanford University, Stanford, California 94305, United States

[‡]SLAC National Accelerator Laboratory, Menlo Park, California 94025, United States

[§]Departments of Chemistry and of Molecular and Cell Biology, and California Institute for Quantitative Biosciences, University of California, Berkeley, California 94720, United States

Supporting Information

ABSTRACT: Hybrid quantum mechanical−molecular mechanical (QM/MM) simulations are widely used in studies of enzymatic catalysis. Until recently, it has been cost prohibitive to determine the asymptotic limit of key energetic and structural properties with respect to increasingly large QM regions. Leveraging recent advances in electronic structure efficiency and accuracy, we investigate catalytic properties in catechol *O*-methyltransferase, a prototypical methyltransferase critical to human health. Using QM regions ranging in size from reactants-only (64 atoms) to nearly one-third of the entire protein (940 atoms), we show that properties such as the activation energy approach within chemical accuracy of the large-QM asymptotic limits rather slowly, requiring approximately 500−600 atoms if the QM residues are chosen simply by distance from the substrate. This slow approach to asymptotic limit is due to charge transfer from protein residues to the reacting substrates. Our large QM/MM calculations enable identification of charge separation for fragments in the transition state as a key component of enzymatic methyl transfer rate enhancement. We introduce charge shift analysis that reveals the minimum number of protein residues (approximately 11−16 residues or 200−300 atoms for COMT) needed for quantitative agreement with large-QM simulations. The identified residues are not those that would be typically selected using criteria such as chemical intuition or proximity. These results provide a recipe for a more careful determination of QM region sizes in future QM/MM studies of enzymes.

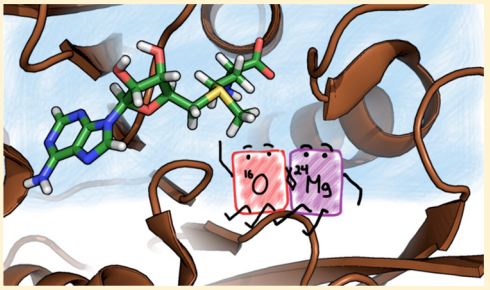

1. INTRODUCTION

A firm understanding of how enzymes facilitate chemical reactions is key for designing molecular catalysts[1] and novel enzymes.[2] Atomistic simulations of enzymes[3] can provide valuable insight by distinguishing rate enhancements due to static, local transition-state stabilization[4] from more nonlocal effects.[5] However, there remains considerable uncertainty regarding the role of the greater protein.[6−10] Enzyme simulation requires a balance of sufficient accuracy to describe chemical rearrangements and catalytic enhancement with low computational cost to enable extensive sampling. Typically, this balance is achieved through a multilevel approach,[11−17] wherein the region of primary interest is treated quantum mechanically (QM), while the surrounding portion of the enzyme is described with an empirical molecular mechanics (MM) model. Largely because of computational limitations, typical QM region sizes (i.e., ligands and a few direct residues) are on the order of tens of atoms.[18−20] There has been much work[17,21−30] to minimize QM/MM boundary effects that might be of concern with small QM regions and to evaluate[31] how advanced, i.e., polarizable,[32,33] force field treatments may improve QM/MM descriptions. However, the requirement to treat crucial[34,35] charge transfer across the QM/MM boundary indicates that boundary-effect minimization and force field adjustment may be insufficient to address the shortcomings of small QM/MM calculations.

Recent advances[34,36−43] in computational efficiency enable fully ab initio, quantum chemical simulation of polypeptides[36] as well as QM/MM treatments of enzymes using ab initio QM methods with large (more than 100 atoms) QM regions. At the same time, advances in the accurate treatment of exchange within range-separated hybrids in density functional theory (DFT) have led to first-principles methods that can reach quantitative agreement with experiment even for nonreactive problems where carefully fit force fields were once thought to be superior (e.g., in properties of water[44]). Despite these advances, studies of the extent to which quantum effects (e.g., due to polarization or charge transfer) are relevant in enzyme catalysis beyond a small active site region have largely been restricted to semiempirical QM/MM methods due to computational cost.[45,46] Thus far, ab initio QM/MM convergence studies have reported disappointingly slow approach to asymptotic limits for NMR shieldings,[47,48] solvation effects,[49] barrier heights,[50,51] excitation energies,[52] partial charges,[53] and

Received: August 2, 2016
Revised: September 9, 2016
Published: October 5, 2016

DOI: 10.1021/acs.jpcb.6b07814
J. Phys. Chem. B 2016, 120, 11381−11394

redox potentials.[54] Computational considerations have restricted these studies to (i) focus on convergence properties in the context of single point energies of one or few structures[41,47,48,55] and (ii) employ local,[53] semilocal,[50,56−59] or global hybrid[48,54] exchange correlation (xc) functionals in DFT. Although it has been possible to carry out one-shot, single point energies of very large systems for some time,[60−66] systematic transition state determination and intermediate geometry optimization, which can require thousands of such single point energies, have been addressed in very few[50,56] QM/MM convergence studies. Additionally, all but one[52] of these studies have been carried out with DFT xc functionals that lack asymptotically correct exchange, producing well-known errors[67−71] in energetics[68,72−76] that likely increase with system size. Thus, the extent to which slow QM/MM region convergence is a consequence of errors in the xc approximation versus the result of an increasingly complete treatment of the chemical environment is still unknown.

In this work, we harness recent advances in computational efficiency with asymptotically correct DFT xc functionals to investigate the convergence of key catalytic properties with increasing QM region size using the model system, catechol *O*-methyltransferase (COMT).[77] COMT regulates neurotransmitters in the human body by transferring a methyl group of *S*-adenosyl-L-methionine (SAM) to deprotonated catecholamines[78] such as dopamine. Methyl transfer is a critical reaction for human health both in neurotransmitter regulation by COMT and in the related DNA methyltransferases[79,80] that regulate gene expression. Unlike in the metalloenzymes that have been the near-exclusive focus of previous QM/MM convergence studies,[50,54,56−59] the reacting substrates in COMT are not covalently bound to the protein. Thus, COMT represents a unique opportunity to decouple boundary effects on QM/MM convergence from effects due to increasingly complete treatments of charge transfer and polarization.

All available COMT crystal structures indicate an unusually short SAM C to catecholate O nonbonded distance of 2.45−2.8 Å, in disagreement with classical molecular dynamics simulation[81,82] and most previous QM/MM simulations[7,83,84] which were limited to small QM regions. The crystal structure also indicates strong bidentate coordination of catecholate to an active site Mg^{2+} that is known from biochemical observations to be essential[77,85] for COMT function. However, previous QM/MM simulations have predominantly indicated a preference for weaker monodentate[86−88] or no coordination[7,84] between Mg^{2+} and catecholate. One possible cause for these discrepancies is the frequent exclusion of Mg^{2+} from the QM region.

Thus, COMT provides (i) a valuable test case for enlarging present understanding of region-size sensitivity in QM/MM simulations and (ii) a representative model enzyme for which electrostatics and charge transfer are expected to be mechanistically critical but are still not well understood. In this work, we systematically determine how properties of reacting substrates at the active site of COMT such as energetics, partial charges, and structural properties approach asymptotic limits with increasingly expansive quantum mechanical descriptions in QM/MM simulations. This allows us to address both methodological questions about QM region sizes in QM/MM and mechanistic questions about COMT reactivity. The outline of the rest of this work is as follows. In section 2, we summarize the computational details, and in section 3, we outline our QM/MM convergence approach. In section 4, we present results and discussion on (i) the convergence of key properties with increasingly large QM/MM models, (ii) mechanistic insight afforded by large QM/MM models, and (iii) an approach for systematic determination of atom-economical QM regions in QM/MM calculations. Finally, in section 5, we provide our conclusions.

2. COMPUTATIONAL DETAILS

Our simulation preparation starts from the crystal structure of the soluble, human form of COMT[89] (PDB code 3BWM, structure shown in Figure 1), which has been solved in the presence of a dinitrocatecholate (DNC) inhibitor. Six residues at the C terminus and one residue at the N terminus of the protein are unresolved in the crystal structure, producing a 214-residue, 3419-atom model, where the first and last resolved residues were treated as the N and C termini, respectively, during preparation by the tleap utility. We converted DNC to a catecholate anion (CAT) substrate in the COMT structure by removing the nitro groups, and we preserved three resolved buried water molecules (of 110 total crystal waters resolved in 3BWM, the remainder of which were adjacent to the external surface of the protein) near the catalytically relevant Mg^{2+} ion (HOH411, HOH402, and HOH403 in 3BWM). All other external water molecules were later replaced during solvation of the complete protein. The protein was protonated using the H++ Web server,[90−92] assuming a pH of 7.0, which yielded a holoenzyme net charge of −6. Neutralizing Na^+ charges were added using the AMBER tleap program.[93] Counterions introduced to produce a neutral simulation cell were always treated with the force field. Generalized Amber force field (GAFF) parameters were determined for both SAM and catecholate using the Antechamber code in AMBER for use alongside the ff12SB force field for the rest of the protein in MM simulations.[93] For MM simulations, a truncated octahedron with 15 Å buffer of water from the edge of the protein before *NPT* equilibration was employed with periodic boundary conditions.

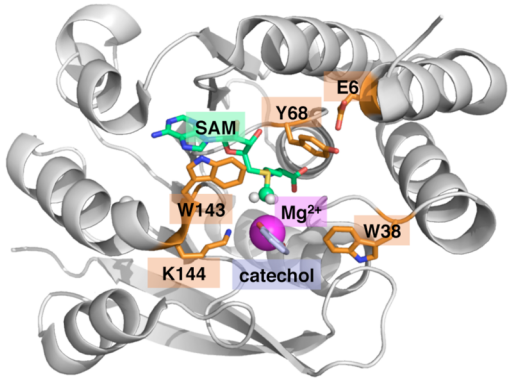

Figure 1. COMT protein with active site features highlighted. The reactants (SAM and catechol) are shown in green and purple, respectively, as well as an Mg^{2+} ion in magenta and five key residues identified from experiments (orange).

Prior to QM/MM simulations, a well-equilibrated MM structure was obtained as follows: (i) 1000 constrained-protein (i.e., only solvent and ions are minimized while the protein is held fixed) and 1000 free-protein minimization steps (i.e., everything in the system is minimized), (ii) 20 ps quick *NVT* heating to 300 K, (iii) 5 ns *NPT* equilibration (p = 1 bar, T =

DOI: 10.1021/acs.jpcb.6b07814
J. Phys. Chem. B 2016, 120, 11381−11394

Table 1. Summary of QM Regions Studied in This Work[a]

region	radius (Å)	no. residues	no. QM atoms	no. link atoms	total atoms	QM charge	min[d(link−COM)] (Å)	n_{link} < 8 Å
1	0.00	0	64	0	64	+2		
2	1.75	3	120	6	126	+2	6.9	1
3	2.00	7	172	14	186	0	5.3	3
4	2.25	13	268	20	288	0	6.7	7
5	2.50	19	387	26	413	+1	6.0	9
6	2.75	22	448	24	472	+1	5.5	7
7	3.00	26	497	24	521	+1	7.5	5
8	5.00	34	600	32	632	−1	7.5	4
9	6.00	43	738	28	766	−1	7.5	2
10	7.00	56	940	28	968	−1	10.0	0

[a]Quantities include the model number, radius of the cut used to define the region, number of nonsubstrate or cofactor residues, number of QM atoms, number of link atoms, total number of atoms in the QM calculation (link atoms plus QM atoms), charge assigned to the QM region, the minimum distance between the central reacting atoms (S, C, O) center of mass (COM) and the closest link atom(min[d(link−COM)]), and the number of link atoms within 8 Å (n_{link} < 8 Å) of the COM.

300 K), and (iv) 100 ns of *NVE* production runs. A representative snapshot was selected from the MM production run by choosing a random structure with C−O distance equal to the mode of the C−O SAM−catechol distance distribution (~3.11 Å)[82] for subsequent AMBER-driven QM/MM geometry optimizations and nudged elastic band[94] calculations.

For all QM/MM simulations, we used the TeraChem package[95] for the QM portion and AMBER 12[93] for the MM component. The QM region is modeled with DFT using the range-separated exchange−correlation functional ωPBEh[96] (ω = 0.2 bohr^{-1}) with the 6-31g[97] basis set, a combination we have previously benchmarked for protein structure.[36] In the QM/MM calculations, an aperiodic spherical droplet was extracted from the production MM results by selecting the largest radius (at least 10 Å of solvent) that could be inscribed in the truncated octahedron using the center of mass utility in PyMOL.[98] Comparisons to results obtained by directly starting QM/MM calculations from the crystal structure geometry are provided in the Supporting Information. Voronoi deformation density (VDD) charges[99] were chosen to assess intersubstrate and substrate−protein charge transfer due to their relatively low basis set sensitivity.[99]

3. APPROACH

QM regions were obtained by starting from a model that consisted of only SAM and catecholate substrates and identifying residues that were within increasing cutoff distances from these reactants. We chose a total of 10 QM region sizes for QM/MM calculations ranging from the reactants-only (including the Mg^{2+} ion) model **1** (64 atoms and 0 protein residues in the QM region) to a largest model **10** consisting of 940 atoms (reactants and 56 protein residues in the QM region) (Table 1). Regions were chosen by sequentially increasing the cutoff distance at values of 0.00, 1.75, 2.00, 2.25, 2.50, 2.75, 3.00, 5.00, 6.00, and 7.00 Å from any atom in a residue to any atom in either SAM or catecholate, as determined using determined using distance functions in PyMOL[98] on the crystal structure (Figure 2). These distance cutoffs were chosen to obtain region sizes that differed by around five residues in size for the small to midsized QM regions (the list of residues in each QM region is provided in Supporting Information Table S1). In the two largest regions, two charged residues (D150 and D205) were excluded despite satisfying the distance cutoffs in order to obtain a QM region with a net charge of −1 rather than −3, avoiding challenges for

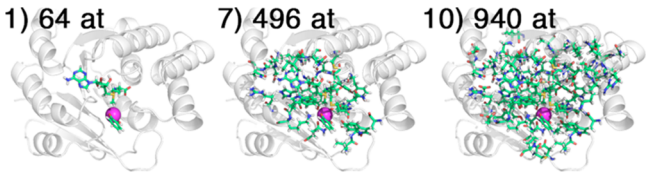

Figure 2. QM regions shown for models **1** (64 atoms, 0 residues), **7** (496 atoms, 26 residues), and **10** (940 atoms, 56 residues) with QM atoms shown in green stick representation.

DFT with highly charged anionic systems.[100−102] Notably, D150 and D205 were not covalently bound to any other residues in the QM region, and their exclusion thus reduced the number of covalent bonds spanning the QM/MM boundary from 32 to 28. The charge for each QM region, including contributions from both residue protonation state and substrate charge states, ranges from a net charge of +2 for the minimal QM model **1** up to −1 for the largest model **10** (Table 1).

The range of sampled QM regions was chosen in part in order to study the effect of incrementally incorporating residues that complete the Mg^{2+} coordination sphere (axial water, D141, D169, and N170) or were observed experimentally to have a significant role on catalytic efficiency (E6, W38, Y68, W143, and K144; see Figure 1).[9] Some of these experimentally identified residues may contribute more directly to dynamic effects and structural stability (e.g., the W38 and W143 "gatekeeper"[78] residues that are believed to facilitate substrate binding), whereas our geometry optimizations and reaction pathway analysis should identify residues with the largest electrostatic effect. The Mg^{2+} coordination sphere residues are sequentially incorporated: D141 into model **3** and larger, N170 in model **5** and larger, and D169 in model **8** and larger. Of the experimentally relevant residues, models **2** and **3** include only K144, models **4** and **5** incorporate also Y68, and models **6** and **7** further include W38 and W143 in the QM region. Only the largest models (**8**−**10**) incorporate E6, which forms a hydrogen bond with the SAM-proximal residue Y68. Additionally, up to three water molecules resolved in the active site crystal structure were included in the QM region size sequentially as one water molecule in models **2**−**4**, two water molecules in model **5**, and all three water molecules in models **6** and larger. None of the external water molecules solvating the protein were included in the QM region, even if they fell within the radial distance cutoff (e.g., for the largest models).

DOI: 10.1021/acs.jpcb.6b07814
J. Phys. Chem. B 2016, 120, 11381−11394

Although most previous QM/MM convergence studies have focused on radial increases in QM region size around an active site,[55,57−59] some alternative schemes have been recently suggested for constructing large QM regions including (i) chemical motivation (e.g., hydrogen bonding interactions and close contacts),[54] (ii) free energy perturbation analysis,[56] or (iii) charge deletion analysis.[50] A motivating factor for radial QM region selection is to avoid biasing QM region choice by incomplete chemical intuition. By sequentially incorporating electronic structure effects from increasingly remote residues, we may identify whether a quantum mechanical treatment of these residues is required or if a force field description is sufficient. We will also later show that our largest QM region results may be analyzed to determine which residues participate in charge transfer events along the reaction coordinate, permitting identification of the fewest number of QM residues needed for converged QM/MM properties.

The final questions pertain to the choice of xc functional and basis set to be used. There is now ample evidence that many commonly used xc functionals are poorly suited to large quantum mechanical regions. For example, closure of the highest-occupied/lowest-unoccupied molecular orbital (HOMO−LUMO) gap using semilocal and global hybrid xc functionals has been observed in numerous insulating systems such as polypeptides, proteins, and solvated molecules.[40,103−105] Extending these previous observations, we find that the QM/MM HOMO−LUMO gap for COMT obtained with global hybrids (e.g., B3LYP[106−108]) closes for QM regions 13 residues and larger (model **4**, see Supporting Information Figure S1). Since a constant 4 eV gap is maintained for all larger models with ωPBEh,[96] all simulations in this work use this range-separated hybrid (ω = 0.2 bohr^{-1}). Regarding basis set, despite recent advances in both hardware and electronic structure methodology, complete basis set limit calculations at the system sizes studied in this work are still well beyond current capabilities. In order to circumvent this limitation, we select a modest 6-31G basis set that has previously been demonstrated to provide good relative energetics and structural properties in protein structure,[36] and we again focus here on relative energetic and structural properties.

4. RESULTS AND DISCUSSION

4a. QM/MM Convergence of ES Complex Properties. We now consider the convergence of properties that underlie enzyme catalysis in catechol *O*-methyltransferase with increasing QM region size in QM/MM simulations. Numerous crystal structures of COMT[89,109−114] have highlighted unusually short SAM methyl to catecholate oxygen (C−O) distances of approximately 2.45−2.8 Å in the reactant enzyme−substrate (ES) complex. We carried out structural optimizations, in each case starting from the same 3.11 Å C−O distance well-equilibrated MM structure (see Computational Details) across our 10 different QM region models. We observe significant shortening of the C−O distances over observed values in solution[115] or classical MD,[81,82] particularly when more residues are introduced into the QM region (Figure 3). In total, C−O distances are reduced by around 0.3 Å with increasing QM region size, from about 3.15 Å in the reactants-only model **1** to 2.85 Å in the largest model **10** with comparable results for model 7 (~500 atoms, 26 residues; a full list is provided in Supporting Information Table S1) and larger. Similar distance reduction is observed for structural optimizations starting from the crystal structure, with distances as short as 2.65 Å favored in the largest QM models (see Supporting Information Figure S2). Differences in results for the two geometry optimizations are likely due to differences in protein structure favored by the MD simulations and the solved X-ray crystal structures, respectively, but the trends are comparable. This reduced distance is consistent with shortened distances in a number of COMT crystal structures[89,110,113] and is at variance with previous predictions from classical MD treatments[81,82] or quantum mechanical studies with restricted QM regions.[7,83,84]

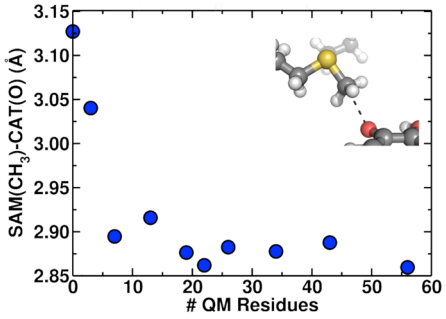

Figure 3. Dependence of reactant distances in the protein (distance from transferring methyl carbon of SAM to acceptor oxygen of catecholate) on QM region size. QM region sizes are reported in terms of the number of protein residues included in each QM region from reactants-only (0 residues, 64 atoms) to a 7 Å radius around the reactants (56 residues, 940 atoms). Inset shows the orientation of the methyl donor and acceptor.

It is often thought that the accuracy of a given choice for the QM/MM boundary might be affected by the charge state of the QM region (with charge neutrality being preferred) and/or the number of covalent bond cuts connecting the QM and MM regions. In the present work, we do not find a high degree of correlation between these characteristics of the QM region and the accuracy of the resulting QM/MM treatment. For example, changes in the net charge of the QM region cannot explain the variation in distance: the charge differs between models **2** and **3** (from +2 to 0) but the C−O distance continues to decrease for models **5** and **6** where the net charge is 1. In order to assess boundary effects, we computed the minimum distance (min[d(link−COM)]) between any link atom and the center of mass (COM) of central SAM (S, C) and catecholate (O) atoms. For all intermediate regions **2**-**6**, min[d(link−COM)] values range from 5.3 Å in model **3** to 6.9 Å in **2**, and this distance increases to 7.5−10.0 Å for the largest models (Table 1). Overall, the proximity of a link atom does not correlate with the distance changes. The largest total number of link atoms closer than 8 Å to the COM (n_{link}) is 9 for region **5**, but the optimal C−O distance obtained for this region is in reasonable agreement with the asymptotic limit obtained in larger QM regions. Thus, these results suggest that incorporating more atoms into the QM region does not simply dampen a size or boundary effect. In fact, COMT represents a special case because boundary effects from cutting through covalent bonds in QM/MM regions[17] should be the smallest in the reactants-only model where there are no covalent bonds spanning the QM/MM boundary, and the large reactant size means that most nonminimal model boundaries are distant from the reacting atoms' COM. Here, our results suggest that specific effects on charge density and polarization of the reactants are only converged when a number of remote residues are treated more flexibly (i.e., quantum mechanically).

DOI: 10.1021/acs.jpcb.6b07814
J. Phys. Chem. B 2016, 120, 11381−11394

As a metric for differences in the substrate electronic structure as QM region size is increased, we evaluated VDD partial charges for these same optimized ES complexes. In isolation, catecholate (CAT) is a singly charged anion; SAM is positively charged with a S^+-CH_3 moiety as well as a positively charged NH_3^+ proximal to a negatively charged terminal carboxylate (see Figure 4 inset). In the smallest model **1**, SAM,

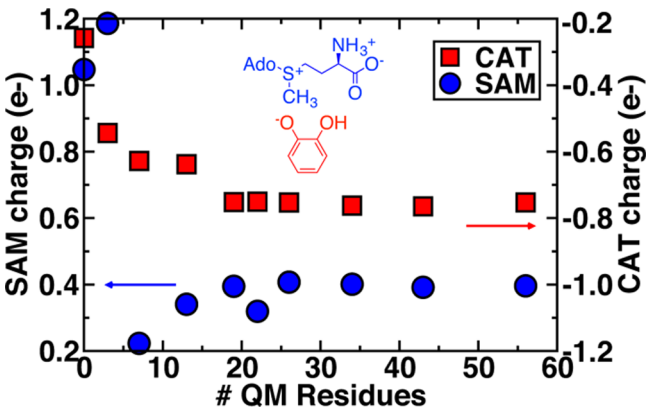

Figure 4. Dependence of partial charges for reactants on QM region size. Charges on SAM (blue circles, blue structure) and catecholate (CAT, red squares, red structure) are compared with the values indicated on left and right *y*-axes, respectively. The scale of the *y*-axis is the same for SAM and CAT, but the charges are of opposite sign (positive for SAM and negative for CAT).

CAT, and Mg^{2+} (i.e., the entire quantum region) are assigned a total charge of +2, whereas the charge constraint on the active site is relaxed in larger models. The total charge of the SAM and CAT moieties (determined by summing partial VDD charges for atoms in SAM and CAT) slowly approach an asymptotic limit with increasing QM region size (Figure 4) consistent with previous observations for the C−O distance (see Figure 3). SAM partial charges are not monotonic, at first increasing to as much as +1.2 *e* for model **2** from +1.0 *e* for model **1** and then rapidly decreasing to +0.2 *e* in model **3** followed by a slow increase to an asymptotic limit around +0.4 *e* for model **7** (26 residues, ∼500 atoms) and larger.

The overall change in charge with QM region size appears to be mediated by charge transfer between the SAM carboxylate and neighboring hydrogen bonding residues (e.g., E90, S72, S119, and H142) that are treated quantum mechanically only in models **3**−**5** and larger (see section 4d). This environment stabilizes the donating sulfur, coinciding with an elongation in the S^+-CH_3 bond by about 0.1 Å. For catecholate, the partial charge changes monotonically with growing QM region size, increasing from −0.25 *e* in the minimal model **1** to an asymptotic limit of around −0.75 *e*. The increased negative charge on catecholate, as mediated by the surrounding protein environment, would increase electrostatic attraction to the positively charged SAM methyl group and thus promote C−O distance reductions in larger QM models. Overall, our results suggest that the fundamental electronic structure description of the reactants is altered when surrounded by a quantum mechanically described protein environment rather than an MM point charge description. The implication of charge transfer also suggests that polarizable force fields would not substantially reduce QM region sensitivity, consistent with some recent observations for polarizable embedding in QM/MM.[31]

4b. Reaction-Coordinate Dependence of QM Region Convergence. We have shown that the description of the ES complex changes substantially when we increase QM region size. The evolution in electronic structure properties of reactants with increasing quantum mechanical treatment of the protein environment suggests that reactivity may also be modified. In order to confirm this hypothesis, we consider how activation energies and reaction energetics for the rate determining methyl transfer step in COMT vary with increasing QM region size (Figure 5). Methyl transfer

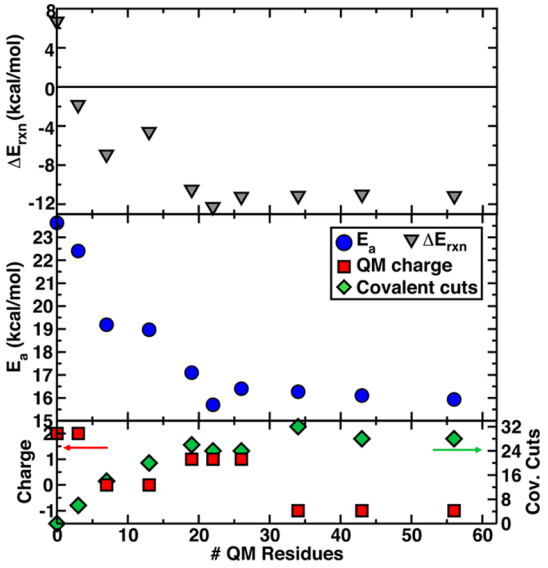

Figure 5. Dependence of methyl transfer reaction enthalpy (top) and activation energy (middle) on QM region size compared to (bottom) variation in charge of QM region (red squares) and number of covalent cuts in QM region (green diamonds) with increasing region size.

activation energies (E_a) decrease nearly monotonically from 24 kcal/mol in the minimal model **1** to an asymptotic limit of 16 kcal/mol once 26−30 or more protein residues are included in the QM region. This behavior is similar to the QM region size dependence of C−O distance and CAT/SAM charge shown in Figures 3 and 4. Although we have not incorporated entropic effects here to give a direct comparison to the $\Delta G^{\ddagger}$ (=18 kcal/mol)[116] obtained from experiments ($k_{cat} \approx 24$/min),[9,116] we would expect the enthalpic barrier to be slightly lower. Thus, we obtain near-quantitative agreement of large-scale QM/MM methyl transfer barriers obtained with range-separated hybrids without need for ad hoc corrections, e.g., due to the use of semiempirical[7] or semilocal exchange−correlation functionals.[117] More importantly than quantitative agreement alone that may be sensitive to basis set choice, important qualitative changes are observed. As the QM region size is increased, the reduction in reactant distances and charge adjustment on the ES complex increases the similarity in the TS and ES structures and reduces the reaction barrier.

The methyl transfer reaction enthalpy (ΔE_{Rxn}) also changes nearly monotonically with increasing QM region size (Figure 5, upper panel), corresponding to increasingly favorable reaction energetics as the QM region is enlarged. Variations in the number of covalent cuts at the boundary or the overall charge of the QM region appear to have little effect and do not correlate with changes in activation energy or reaction energy

DOI: 10.1021/acs.jpcb.6b07814
J. Phys. Chem. B 2016, 120, 11381−11394

(Figure 5, lower panel). The minimal model reaction energy is predicted to be weakly endothermic, consistent with previous smaller QM region QM/MM results[86,117,118] on COMT. Instead, the asymptotic limit ΔE_{Rxn} = −11 to −12 kcal/mol is reached at around model **6** (22 residues). The underestimation of reaction favorability with small QM regions can likely be ascribed to Mg^{2+} coordination: as bidentate catecholate is methylated, its strength as a chelator to Mg^{2+} is weakened. For the small QM regions, Mg^{2+} coordination is mixed between QM and MM residues, with the stabilization by pure MM residue coordination likely insufficient with respect to QM residues because it does not allow for charge transfer. Therefore the effect of weakening coordination during methylation is overestimated in smaller QM region models. QM region size impacts both quantitative predictions and qualitative aspects of the COMT methyl transfer mechanism. Currently, free energy barriers computed on the largest QM region sizes studied in this work (approximately 600−1000 atoms) are prohibitive, but we expect that the smaller overall magnitude of entropic contributions to the QM region barrier means that the entropic difference for differing region sizes is likely a substantially smaller contribution than the 8 and 20 kcal/mol differences observed for the activation energy and reaction enthalpy, respectively, from the smallest to the largest QM model.

Although numerous studies have been carried out in evaluating how energetics approach their asymptotic limit with increasingly larger QM-only or QM regions in QM/MM calculations,[50,55−59] none have identified whether geometrical properties of both the reactants and the transition state (TS) converge at similar rates with QM region size. Crystal structures of COMT[89,109−114] all feature unusually short C−O distances, and experimental measurements of kinetic isotope effects[9,82,119] have been suggested by some[120] to be indicative of unusually short C−O or S−O distances in the transition state as well. Here, we identify the transition state approximately as the highest energy structure obtained along the NEB reaction path. In order to compare TS structures for all QM/MM models, we compare both absolute TS geometrical properties, i.e., (i) the distance of the methyl donor SAM S to methyl group C, d(S−C), and (ii) the distance of the methyl acceptor CAT O^- to methyl group C, d(C−O), as well as relative differences between the TS and the ES complex. Unlike the nonbonded reactant C−O distance (Figure 3), the TS C−O distance shows nonmonotonic behavior with increasing QM region size. For QM models **1**−**3**, the C−O distance reduces significantly from ∼2.0 Å to ∼1.8 Å (Figure 6). At the same time, the S−C distance lengthens (from 2.3 to 2.4 Å), which would lead to identification of a much later transition state if model **3** were used for mechanistic study. This trend reverses with first lengthening of C−O distances from models **3** to **7** leveling off at around 2.1 Å and a shortening of the S−C distance to about 2.25 Å for the three largest models. In all cases, d(S−C) is longer than d(C−O) in the TS, but the difference is largest in small QM models and is reduced for the larger models. Key relative geometric properties between the TS and ES complex include SAM S−CAT O^- distance differences,

$$\Delta(\text{S}-\text{O}) = d(\text{S}-\text{O})|_{\text{TS}} - d(\text{S}-\text{O})|_{\text{ES}} \quad (1)$$

and the lengthening of the S−C bond in the transition state from its equilibrium value,

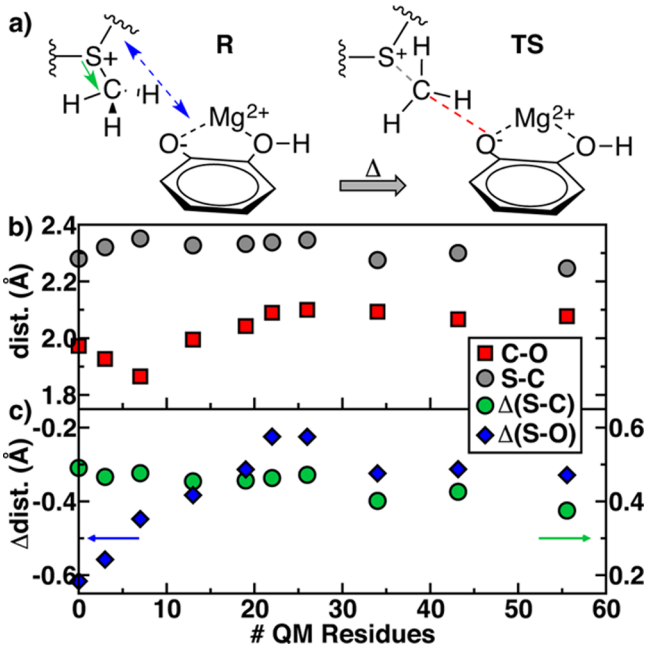

Figure 6. Enzyme−substrate complex reactant (R) and transition state (TS) structures annotated with TS−R Δ(S−C) distance and TS−R Δ(S−O) distance (left) and S−C or C−O distance (right). (b) S−C (gray circles) and C−O (red squares) distances with QM region size. (c) TS−R Δ(S−C) distance (green circles) and TS−R Δ(S−O) distance (blue diamonds) with QM region size.

$$\Delta(\text{S}-\text{C}) = d(\text{S}-\text{C})|_{\text{TS}} - d(\text{S}-\text{C})|_{\text{ES}} \quad (2)$$

Recall that ES complex d(C−O) and thus d(S−O) are monotonically reduced with increasing QM region size (Figure 3). In the TS, the substrate distances, as monitored by d(S−O), are even shorter. However, the TS geometry is not affected by QM region enlargement in a manner comparable to the ES complex. Therefore, the relatively large Δ(S−O) of −0.6 Å in the smallest model instead levels off around −0.3 Å for QM/MM models **8**−**10**. That is, large QM treatments impact the TS geometry less, and the enlargement of the QM region causes the ES complex structure to become more transition-state-like. This observation is reinforced by Δ(S−C), which also decreases from 0.5 Å to under 0.4 Å. Such a result suggests that the strong dependence of methyl transfer activation energies on QM region size (Figure 5) arises from a lack of cancellation of errors between the ES complex and the TS. These observations reinforce the need to study QM/MM model convergence at multiple points along the reaction coordinate, which has only occasionally been carried out.[50]

Geometric analysis of the ES complex and transition state (TS) has revealed differences in sensitivity to QM region definition. Substrate partial charge analysis in the ES complex (see Figure 4) suggests that QM region sensitivity in COMT is at least somewhat due to charge transfer between the substrates and the surrounding protein. At the transition state, the formal charge on either substrate fragment is likely to be smaller, and thus we investigate whether the TS partial charges show altered QM region size sensitivity compared to the ES complex reactants, R. We quantify the charge transfer from the substrates to the environment in two ways: (i) the core substrate partial charge, which is the partial charges summed over both SAM and catecholate, and (ii) the Mg^{2+} partial charge. Together, (i) and (ii) must be equal to +2 for our

DOI: 10.1021/acs.jpcb.6b07814
J. Phys. Chem. B 2016, 120, 11381−11394

minimal model **1** but could deviate from this idealized value for larger models. Indeed, as the QM region size is increased, both TS and R core and Mg^{2+} partial charges become much more neutral with net overall charges approaching an asymptotic limit around −0.20 to 0.25 *e* for the TS and −0.30 to 0.35 *e* for R (Figure 7). The partial charge on Mg^{2+} (Figure 7)

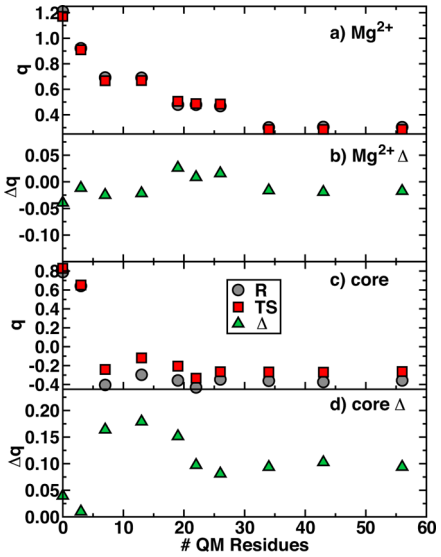

Figure 7. (a) Reactant (R) and transition state (TS) partial charges and (b) TS−R partial charge differences for Mg^{2+}. (c) R and TS partial charges summed over the core (SAM and catecholate only) and (d) TS−R differences for the core.

approaches an asymptotic limit of around 0.3 *e* even more slowly at model **8** but in a similar fashion for both R and TS. This trend in Mg^{2+} charge appears to be derived from inclusion of the Mg^{2+} coordination sphere residues in the QM region.

It is useful to compare whether the difference in the partial charges in the reactant and transition state, Δq(TS−R), converge faster than absolute charges alone through cancellation of errors. For the smallest regions **1** and **2**, the core Δq(TS−R) is constrained by limited region size to be nearly zero, but the TS becomes relatively more positive by up to 0.20 *e* for intermediate regions **3**−**5**. A loss of 0.1 *e* from the R core to the TS is observed for models **7** and larger, consistent with the slow approach to a constant value observed in properties of the ES complex alone. The Mg^{2+} Δq(TS−R) similarly approaches a constant value at around −0.025 *e* for model **8** and larger. Although the difference in the R and TS Mg^{2+} partial charge is small, it does change sign (e.g., from model **4** to model **5**), indicating high sensitivity to the surrounding environment. From either the perspective of the reacting substrates or Mg^{2+} cosubstrate, differences in the electronic environment between the R and TS do not benefit from cancellation of errors, explaining the slow approach to asymptotic limits of reaction energetics.

4c. Mechanistic Insight from Large-Scale QM/MM Reaction Pathway Analysis. Using the large QM region model **10**, we may identify how substrate partial charges evolve along the methyl transfer reaction coordinate (Figure 8). First, we approximate the reaction coordinate (Δ) by the difference in the SAM sulfur methyl donor distance to the methyl carbon (d(S−C)) and the catecholate oxygen methyl acceptor distance to the methyl carbon (d(C−O)):

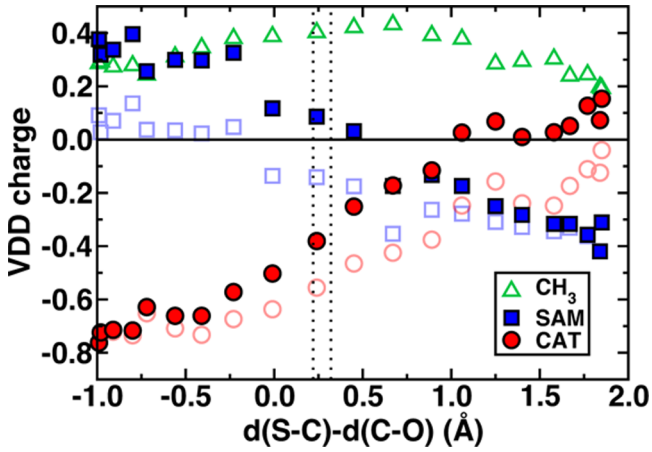

Figure 8. By-residue partial charges of SAM (blue filled squares) and catecholate (CAT, red filled circles) along the reaction coordinate defined by the difference in the distance of the transferring methyl carbon to the donor SAM S atom and the acceptor catecholate O atom, as described in the main text. The transition state region is shown as two vertical dotted lines. For comparison, sums of the charge over the methyl group only (green open triangles), adohomocysteine (blue open squares), and unmethylated catecholate (red open circles) are also shown.

$$\Delta = d(\mathrm{S{-}C}) - d(\mathrm{C{-}O}) \tag{3}$$

Values of Δ obtained from the model **10** reaction coordinate are provided in Supporting Information Table S2. In order to sum charges along this reaction coordinate, we recall that the methyl group transfers from SAM to catecholate with O-methylated catechol (OMC) and AdoHomocysteine (AdoHcy) as the products. Therefore, we subdivide the partial charge on the methyl group (green open triangles in Figure 8) between the SAM/AdoHcy (q_S) and CAT/OMC (q_C) fragments according to the relative position, i, of the methyl group along the reaction coordinate, Δ, between reactant (R) and product (P) states:

$$q_S^i = q_{\mathrm{AdoHcy}}^i + q_{\mathrm{CH_3}}^i \left[\frac{\Delta(\mathrm{P}) - \Delta(i)}{\Delta(\mathrm{P}) - \Delta(\mathrm{R})} \right] \tag{4}$$

and

$$q_C^i = q_{\mathrm{CAT}}^i + q_{\mathrm{CH_3}}^i \left[\frac{\Delta(i) - \Delta(\mathrm{R})}{\Delta(\mathrm{P}) - \Delta(\mathrm{R})} \right] \tag{5}$$

These partitioned charges and results from alternative partitioning schemes are provided in Supporting Information Table S3. At the highest energy point identified along the reaction coordinate for model **10**, Δ is ∼0.32 Å, close to the point (Δ = 0.40 Å) where the methyl group partial charge is equally divided between q_S and q_C. Analysis of the CAT/OMC partial charges at the transition state reveals that the methyl acceptor is still somewhat reactant-like with a negative charge of around −0.4 *e* even after including half of the highly partially charged methyl group (+0.4 *e*, the unmethylated CAT partial charges are shown in open circles in Figure 9). Similarly, SAM partial charges remain weakly positive even at the transition state (+0.1 *e*) and are not substantially changed with respect to the reactant structure.

Considering even further the close-range interaction between the methyl acceptor on catecholate and the transferring methyl group, electrostatic attraction between the two species (+0.4 *e*

DOI: 10.1021/acs.jpcb.6b07814
J. Phys. Chem. B 2016, 120, 11381−11394

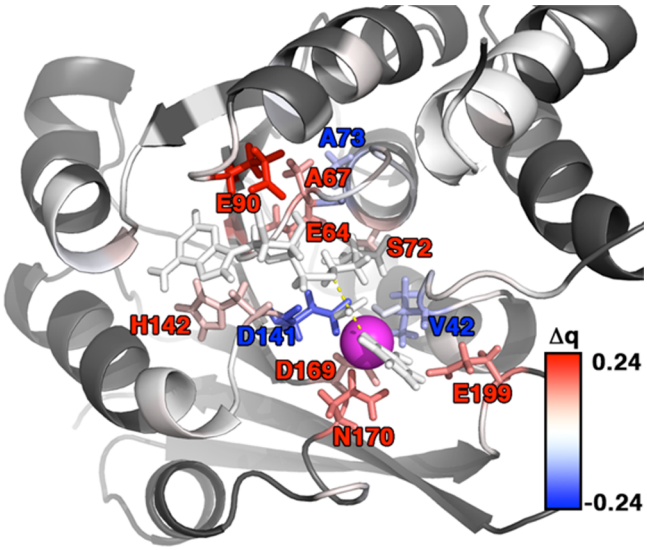

Figure 9. Difference of by-residue VDD charge sums upon removal of the substrates (SAM, catecholate, and Mg^{2+}) with substrates in transition state structure shown in white sticks. Residues shown and labeled in blue lose partial charge upon substrate removal, whereas residues shown and labeled in red gain partial charge upon substrate removal (as shown in inset color bar). All residues with $\Delta q \geq |0.05|$ are shown as sticks. All remaining QM residues are shown in cartoon as white, whereas MM residues are shown in dark gray.

for the methyl group, −0.6 *e* for the unmethylated catecholate) is still substantial at the transition state. Later in the reaction coordinate ($\Delta \approx 0.75-0.9$) SAM becomes negatively charged, and the catecholate is neutralized only for $\Delta > 1.0$ Å. This range of $\Delta = 0.75-1.0$ Å corresponds to $d(S-C) > 2.50$ Å and $d(C-O) < 1.75$ Å, which is a near product-like state in terms of both geometry (in the products, $d(C-O) = 1.44$ Å) and energetics. Thus, earlier suggestions[7,86] that electrostatic attraction in the reactants is annihilated at the transition state is apparently an oversimplification when charge transfer is permitted between substrates and the enzyme.

Comparison to minimal model **1** reveals that constraining the charge on SAM, catecholate, and Mg^{2+} to +2 for the entire reaction will produce a positively charged catecholate acceptor at the transition state (+0.1 *e*, see Supporting Information Figure S3). The net +2 charge in the QM system is distributed over Mg^{2+} (+1.2 *e* in the reactants) and SAM (+1.0 *e* in the reactants), but this leaves little room for CAT to accumulate a strong negative charge (−0.2 *e* in the reactants). Instead, we observe that when this artificial constraint is lifted by enlarging the model, the core substrates (SAM and catecholate) accumulate negative charge from surrounding residues (see section 4b). Thus, the electrostatic attraction between reactants is considerably weaker in the minimal model **1** than the large model **10**, which serves as a possible physical origin for the 8 kcal/mol higher barrier in **1** versus **10**. In model **1**, the non-methyl part of CAT becomes positive in the product state (+0.3 *e*, +0.6 *e* with the methyl group), thus making it a very poor chelator to Mg^{2+}, also explaining the endothermic reaction energy observed earlier for the minimal model (compared to exothermic reaction energy for the large model, as discussed in section 4b). These results suggest that the enzyme, and Mg^{2+} in particular, mediates charge transfer between the reactants and the environment, extending the portion of the reaction coordinate over which electrostatic interaction between the two fragments is favorable past the transition state.

4d. Obtaining Atom-Economical QM Regions. Following confirmation that key properties of the COMT enzyme are consistent for large radially cut QM regions (approximately 600−1000 atoms) in QM/MM calculations, we now aim to identify the subset of residues included in these QM regions that impact reaction coordinate properties most strongly. COMT is a challenging system for QM/MM convergence studies because the SAM, catecholate, and Mg^{2+} substrates alone span a large portion of the protein's solvent-exposed active site, and residues proximal to one substrate may be distant from another. As noted previously (see Figure 7), the core substrates (SAM, catecholate, and Mg^{2+}) carry more negative partial charge than expected from nominal charge assignment, and the total charge evolves as the reaction progresses. Therefore, we first identify which residues have a variation in total electron density during the methyl transfer reaction and are thus acting as charge sources or sinks for the substrates. Using the largest model **10** holoenzyme studied in this work, we computed the per-residue VDD partial charge sums, i.e.,

$$q_{\mathrm{res}}^{\mathrm{VDD}} = \sum_{j \in \mathrm{res}} q_j^{\mathrm{VDD}} \tag{6}$$

on each residue (res) in the QM region for 21 snapshots interpolated along the methyl transfer reaction coordinate (see Supporting Information Tables S4−S7). Total charges of some residues appear to vary strongly, e.g., M40 and N41, which accumulate around −0.15 to 0.2 *e* over the course of the reaction coordinate (Supporting Information Figure S4). However, the partial charge of most residues fluctuates across the methyl transfer coordinate, and there is limited correlation between variation and relative proximity to the substrates in the active site (see Supporting Information Figure S5).

In order to isolate the charge fluctuations most relevant to the substrate environment, we removed SAM, catecholate, and Mg^{2+} from each holoenzyme snapshot, forming an apoenzyme, and repeated the summed-over-residue VDD computations (see Supporting Information Tables S8−S11). In both cases, the sum was computed two ways: with link atoms assigned to their respective residue or excluded, and the no link atom data were used here due to lower fluctuations observed in the following analysis (i.e., link-atom-derived charge fluctuations may lead to false positives; see Supporting Information). The residues that display the largest holoenzyme to apoenzyme (holo−apo) charge shift are expected to be essential to the complete description of the electronic environment in the active site, and a point-charge electrostatic description afforded by MM alone should be insufficient. In order to quantify and rank importance of residues by their interactions with substrates, we compute the difference between the apo and holo residue-summed partial charges (q_{res}) and average them over the reaction coordinate as follows:

$$\Delta q_{\mathrm{res,av}} = \frac{\sum_i^n q_{\mathrm{res},i}^{\mathrm{VDD,apo}} - q_{\mathrm{res},i}^{\mathrm{VDD,holo}}}{n} \tag{7}$$

(here, $n = 21$). Thus, residues that lose charge when the substrates are removed have a negative $\Delta q_{\mathrm{res,av}}$, whereas ones that gain charge back have a positive $\Delta q_{\mathrm{res,av}}$.

In total, we find 11 residues with $\Delta q_{\mathrm{res,av}}$ at least 0.05 *e* in magnitude (Figure 9). These 11 residues include (i) hydrogen

DOI: 10.1021/acs.jpcb.6b07814
J. Phys. Chem. B 2016, 120, 11381−11394

bond acceptors to SAM (E90, E64, H142) and catecholate (E199) that lose substantial charge, (ii) hydrogen bond donors to SAM (S72), (iii) Mg^{2+} coordination sphere residues that alternately lose (N170, D169) or gain charge (D141), and (iv) a cluster of residues behind the SAM substrate that form more indirect interactions (V42, A67, A73). Residues in cases i−iii would have likely been identified with the help of chemical intuition, but other residues that may have been deemed important through chemical intuition arguments alone, e.g., the catechol deprotonating K144, are absent from this list. Similarly, residues that may be key to substrate binding and protein dynamics (e.g., gatekeeper residues W38 and W143) do not impact charge on the substrate and therefore are also not detected by this analysis. Alternatively, proximity may have been a useful strategy for identifying V42, A67, and A73 as relevant residues, since the three residues are adjacent to SAM, but several residues proximal to CAT (e.g., K144, P174, L198) do not show comparable charge sensitivity. The shape of the space occupied by residues with large charge shifts (white and blue sticks shown in inset in Figure 10) is still centered on the

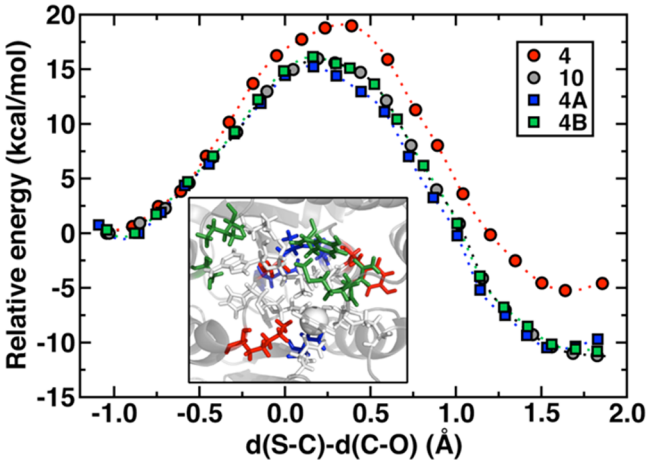

Figure 10. Methyl transfer reaction profiles for original models **4** and **10** (red and gray circles, respectively) and optimized models **4A** and **4B** (blue and green squares, respectively). Inset shows atoms in all QM region models (white sticks), only in model **4** (red sticks), added in model **4A** or **4B** (blue sticks), or added in model **4B** (green sticks). For model **10** QM region, see Figure 2.

substrates but ellipsoidal in nature. Thus, although several of the residues are included in our second or third smallest radial QM regions (V42, E90, D141, N170, E199), others coincide with the intermediate models **4**−**6** (S72, A67, H142) and still others only appear in the larger model **8** (E64, D169, A73) (see Supporting Information Table S12).

An additional five residues (M40, N41, Y68, I91, S119, shown as green sticks in Figure 10 inset) have Δq_{res} that meet or exceed 0.05 *e* in magnitude for at least one snapshot (see Supporting Information Tables S9 and S12). The Mg^{2+}- and catecholate-adjacent residues M40 and N41 have negligible Δq_{res} in the first half of the reaction, but values increase at the transition state and toward the products. Conversely, the Y68 residue, which has been the focus of previous experimental and computational mutagenesis efforts,[9,82] has a large charge shift in the first portion of the reaction but limited effect after the transition state. These five additional residues are present in our original models **3**−**5**. Now, we identify if the results of our charge shift analysis can be used to prune or refine large radial cuts of QM regions in analogy to charge deletion analysis.[50,121,122] Charge deletion analysis has been used[50] with the assumption that any strong QM−MM electrostatic interaction cannot be properly accounted for across the QM/MM boundary, favoring placing that residue in the QM region.[50] Any proximal MM residue with moderately strong point charges will be identified by charge deletion analysis, but we wish to take the more economical view that some QM-point-charge interactions are in fact suitably treated with QM/MM. Thus, we hypothesize that adequate QM regions may instead be constructed on the basis of the residues that exhibit large charge shifts in response to the substrates.

We now construct new QM models from the residues identified in charge shift analysis (CSA) and compare them to the original radial models. Both the 11-residue (214 atoms) and enlarged 16-residue (296 atoms) models are similar in size to model **4** (13 residues, 268 atoms) but comprise different residues. Both of these new models are substantially smaller than the models (7−**8**, 26−34 residues, 497−600 atoms) we previously identified as consistent with the largest model **10** across all properties considered in this work. The 16-residue model omits K144, which appears in our radial models **2** and larger, as well as G66 and Y71, which both appear in radial model **4** (Supporting Information Table S13). All three models have comparable distance (6.4−6.7 Å) between the closest link atom and the center of mass of the S−C−O bond. The new 11- and 16-residue models, which we will refer to as **4A** and **4B**, respectively, reduce the total number of link atoms closer than 8 Å to the S−C−O bond center of mass from 7 in model **4** to 5. The total number of link atoms for **4A** (16) and **4B** (18) is reduced slightly as well from model **4** (20). The omission of K144 and inclusion of a number of anionic residues, however, impart the largest net negative charge to both of these regions (−3) compared to any of the previous radial models (−1).

We computed partial charges and reaction pathways for these new models and compare both to model **4** as a reference for equivalent computational cost as well as to the largest QM/MM model **10** (Table 2). The root sum squared (RSS) error of evaluated residue-summed partial charges (q) for model M with respect to the reference model **10** is evaluated as

$$\mathrm{RSS}(q,\mathrm{M}) = \sqrt{\sum_{\mathrm{res}} (q_{\mathrm{res,M}} - q_{\mathrm{res,10}})^2} \quad (8)$$

In total, we evaluate the (i) reactant (SAM, catecholate, and Mg^{2+}), (ii) transition state (the reactants with CH_3 partitioned as described in section 4c), and (iii) product (AdoHcy, OMC, and Mg^{2+}) partial charges summed over each residue for a total of nine terms in the sum in eq 8. As suggested by sections 4a and 4b, model **4** RSS partial charge error is quite large at 0.7 *e* due to increased partial positive charge on Mg^{2+}, reduced charge separation in the transition state, and enhanced charge separation in the products. The 11-residue and 16-residue models **4A** and **4B**, on the other hand, have good and near-quantitative agreement in partial charges with the larger model **10** with an RSS of 0.3 *e* and 0.0 *e*, respectively. Disagreement for the smaller model is primarily due to increased negative charge on SAM across the reaction coordinate.

We also converged methyl transfer pathways for the **4A**/**4B** models and compute the RSS error in the activation and reaction energies as

$$\mathrm{RSS}(E,\mathrm{M}) = \sqrt{(E_a^{\mathrm{M}} - E_a^{10})^2 + (\Delta E_{\mathrm{rxn}}^{\mathrm{M}} - \Delta E_{\mathrm{rxn}}^{10})^2} \quad (9)$$

DOI: 10.1021/acs.jpcb.6b07814
J. Phys. Chem. B 2016, 120, 11381−11394

Table 2. Properties,[a] Partial Charges,[b], Energetics,[c] and Root Sum Squared (RSS) Errors in Charge and Energy of New Models 4A and 4B alongside Model 4 As Determined by Agreement with the Largest Model 10

	region property					R charge			TS charge			P charge			energetics (kcal/mol)		RSS error	
M	no. residues	no. atoms	no. links	closest	$n < 8$	SAM	CAT	Mg	SAM	CAT	Mg	SAM	CAT	Mg	E_a	ΔE_{rxn}	charge	energy
4A	11	214	16	6.4	5	0.22	−0.67	0.31	−0.01	−0.33	0.32	−0.62	0.09	0.35	15.2	−9.7	0.3	1.6
4	13	268	20	6.7	7	0.34	−0.64	0.69	0.09	−0.21	0.67	−0.76	0.22	0.53	18.9	−4.6	0.7	7.2
4B	16	296	18	6.6	5	0.38	−0.77	0.31	0.13	−0.41	0.29	−0.44	0.10	0.34	16.2	−10.8	0.0	0.4
10	56	940	28	10	0	0.38	−0.76	0.30	0.12	−0.38	0.29	−0.42	0.07	0.34	15.9	−11.2	0.0	0.0

[a]Number of residues, number of QM atoms, number of link atoms, closest link atom (in Å), and number of link atoms, n, within 8 Å. [b]For reactant R, transition state TS, and product P, SAM, CAT, and Mg. [c]Activation energy E_a and reaction energy ΔE_{rxn}.

Using this metric, the radial model **4** has a 7.2 kcal/mol RSS error due to overestimating the barrier height and underestimating reaction exothermicity. In contrast, model **4B** yields near-quantitative agreement of 0.4 kcal/mol RSS error due to sub-kcal/mol differences in barrier height and reaction energetics, and the smaller model **4A** is also in very good agreement with an RSS of 1.6 kcal/mol (Table 2). Comparison of the full methyl transfer reaction profiles (Figure 10) reveals that model **4B** overlaps nearly exactly with model **10**, whereas model **4A** shows a slightly earlier transition state with lower barrier and less exothermic products. However, neither model shows the large deviations apparent between the comparably sized model **4** and the large-scale model **10**, where the full reaction profile highlights again differences in the character of the much later transition state structure as well as qualitative differences in barrier height and shape. Thus, properties consistent with large-QM/MM models may be obtained at a fraction of the computational cost from QM regions with as few as 214−296 atoms as long as the optimal QM residues are selected.

On the basis of these promising results, we propose a general protocol for unbiased QM region determination in QM/MM calculations: (i) partial charges (or other relevant properties[54]) of reacting substrates should be obtained from very large radial models that have no link atoms adjacent to the central active site in reactant, product, and key intermediate or transition-state-like geometries; (ii) the calculations should be repeated with the reacting substrates removed. If the substrates or catalytic center are covalently linked to the protein, mutagenesis rather than complete substrate removal may be necessary, and (iii) the residues for which there is an apparent significant charge or property difference (e.g., 0.05 e or greater difference in charge) from items i or ii should be used to construct a new QM region for QM/MM calculations. (iv) This new QM/MM model may be validated through agreement of energetic, structural, or partial charge properties with the large radial model results. In total, this charge shift analysis requires no more than a handful of very large (∼1000 QM atoms) QM/MM calculations and facilitates a systematic and unbiased determination of an atom-economical QM region that will not require strong chemical intuition nor potentially overestimate electrostatic interactions that are suitably treated across the QM/MM boundary. We also emphasize that the approach is not strongly sensitive to geometric properties by confirming agreement between the results of CSA obtained on the model **10** reactant structure and the small-QM model **1** reactant structure (see Supporting Information Table S14). Given this good agreement, even crystal structures could be a viable option for preliminary analysis, although structural sensitivity to larger protein rearrangements obtained during long-time dynamics is the focus of ongoing work.

5. CONCLUSIONS

We have quantified how key descriptive properties of enzyme catalysis obtained from simulations depend on the size of the QM region in QM/MM calculations for an enzyme in which the smallest possible QM regions typically employed (i.e., SAM and catecholate) do not suffer from boundary effects. Our results on COMT show that geometric and electronic structure properties of the reactants are slow to approach asymptotic limits as remote residues are added radially to the QM region. Namely, both reactant distances and partial charges on reactants converge slowly with increasing QM region size.

DOI: 10.1021/acs.jpcb.6b07814
J. Phys. Chem. B 2016, 120, 11381−11394

Although this result is consistent with nearly a dozen semiempirical and first-principles QM/MM convergence studies that have been carried out in recent years, doubts may still remain in the broader community about the source of this slow convergence regarding the accuracy of the methods employed. By carrying out extensive geometry optimizations and transition state searches with range-separated hybrid DFT made possible through GPU-accelerated quantum chemistry, we have separated substrate property convergence with increasing QM region size from well-known errors of semilocal exchange−correlation functionals in large QM system sizes.

For the COMT example investigated here, radial QM region models that are ∼10× larger than typically used in QM/MM calculations are needed for consistent structural properties or reaction energetics. Although properties such as forces on central QM atoms have been shown to converge only when QM regions were at least 500 atoms in size,[46] it remained possible that error cancellation along a reaction coordinate might instead lead to good prediction of relative properties at smaller QM region sizes. We have instead demonstrated that differences in TS and ES complex property convergence lead to poor cancellation of errors due to differences in charge transfer and residue interactions along the reaction coordinate.

Using our large QM/MM models, we also provided mechanistic insight into the role of the enzyme environment on methyl transfer. Namely, we observed that charge annihilation between the oppositely charged reactants does not occur until after the transition state structure and that the charge transfer between substrates and the protein environment (e.g., Mg^{2+} to its coordination sphere, SAM to E64, E90, E199, and H142) primes the ES complex to be more TS-like.

Finally, we introduced charge shift analysis to pare down large QM models into a minimal set of residues needed for quantitative accuracy. By incorporation of only the residues that participated in charge transfer with the reactants, quantitative agreement with a 56 residue (968 atom) radial QM region was reached with only 16 residues (296 atoms). Although our analysis revealed several residues that might be selected on the basis of chemical intuition (e.g., Y68 or the Mg^{2+} coordination sphere residues N41, D169, N170) or proximity to substrates (e.g., E199), other residues that would have been selected under either criterion from an X-ray crystal structure of COMT, as is standard practice, were identified to be unnecessary (e.g., K144 or Y71). Several nonpolar residues (i.e., V42, A67, and A73) that would have escaped selection using typical criteria were identified as important. Such a technique could provide a useful strategy for circumventing slow convergence obtained based on a typical radial strategy alone (e.g., here only our larger models **8**−**10** completed the Mg^{2+} coordination sphere in the QM region). Ongoing work is aimed toward validating this and related approaches for unbiased determination of optimal QM regions in QM/MM calculations across a range of enzymes and confirming the catalytic role of residues identified through these approaches.

■ ASSOCIATED CONTENT

Supporting Information

The Supporting Information is available free of charge on the ACS Publications website at DOI: 10.1021/acs.jpcb.6b07814.

Details of all QM region model sizes employed; C−O distance region dependence for QM/MM optimizations of 3BWM crystal structure; individual distances along reaction coordinate; partial charge sums over core substrate definitions along reaction coordinate for largest and smallest models; sums per residue with and without link atoms for large QM model; apo−holo charge sum differences with and without link atoms; charge variation plot along reaction coordinate; heat map of residue absolute charge fluctuations (PDF)

PDB coordinates of initial reactant structure, reactants, transition states, and products as well as PyMOL session file for visualizing QM regions (ZIP)

■ AUTHOR INFORMATION

Corresponding Author

*E-mail: todd.martinez@stanford.edu. Phone: 650-736-8860.

Present Address

[‖]H.J.K.: Department of Chemical Engineering, Massachusetts Institute of Technology, Cambridge, MA 02139.

Notes

The authors declare the following competing financial interest(s): T.J.M. is a co-founder of PetaChem, LLC.

■ ACKNOWLEDGMENTS

This work was supported by the Department of Defense (Office of the Director of Defense Research and Engineering) through a National Security Science and Engineering Faculty Fellowship (to T.J.M.) and by National Institutes of Health (NIH) grants to J.P.K. and J.Z. (Grants GM025765 and GM039296). H.J.K. holds a Career Award at the Scientific Interface from the Burroughs Wellcome Fund.

■ REFERENCES

(1) Gao, L.; Zhuang, J.; Nie, L.; Zhang, J.; Zhang, Y.; Gu, N.; Wang, T.; Feng, J.; Yang, D.; Perrett, S.; et al. Intrinsic Peroxidase-Like Activity of Ferromagnetic Nanoparticles. *Nat. Nanotechnol.* **2007**, *2*, 577−583.

(2) Siegel, J. B.; Zanghellini, A.; Lovick, H. M.; Kiss, G.; Lambert, A. R.; St. Clair, J. L.; Gallaher, J. L.; Hilvert, D.; Gelb, M. H.; Stoddard, B. L.; et al. Computational Design of an Enzyme Catalyst for a Stereoselective Bimolecular Diels-Alder Reaction. *Science* **2010**, *329*, 309−313.

(3) Gao, J.; Ma, S.; Major, D. T.; Nam, K.; Pu, J.; Truhlar, D. G. Mechanisms and Free Energies of Enzymatic Reactions. *Chem. Rev.* **2006**, *106*, 3188−3209.

(4) Fastrez, J.; Fersht, A. R. Mechanism of Chymotrypsin - Structure, Reactivity, and Nonproductive Binding Relationships. *Biochemistry* **1973**, *12*, 1067−1074.

(5) Fraser, J. S.; Clarkson, M. W.; Degnan, S. C.; Erion, R.; Kern, D.; Alber, T. Hidden Alternative Structures of Proline Isomerase Essential for Catalysis. *Nature* **2009**, *462*, 669−673.

(6) Villa, J.; Warshel, A. Energetics and Dynamics of Enzymatic Reactions. *J. Phys. Chem. B* **2001**, *105*, 7887−7907.

(7) Roca, M.; Marti, S.; Andres, J.; Moliner, V.; Tunon, I.; Bertran, J.; Williams, I. H. Theoretical Modeling of Enzyme Catalytic Power: Analysis of "Cratic" and Electrostatic Factors in Catechol O-Methyltransferase. *J. Am. Chem. Soc.* **2003**, *125*, 7726−7737.

(8) Olsson, M. H. M.; Parson, W. W.; Warshel, A. Dynamical Contributions to Enzyme Catalysis: Critical Tests of a Popular Hypothesis. *Chem. Rev.* **2006**, *106*, 1737−1756.

(9) Zhang, J.; Klinman, J. P. Enzymatic Methyl Transfer: Role of an Active Site Residue in Generating Active Site Compaction That Correlates with Catalytic Efficiency. *J. Am. Chem. Soc.* **2011**, *133*, 17134−17137.

(10) Klinman, J. P.; Kohen, A. Hydrogen Tunneling Links Protein Dynamics to Enzyme Catalysis. *Annu. Rev. Biochem.* **2013**, *82*, 471−496.

DOI: 10.1021/acs.jpcb.6b07814
J. Phys. Chem. B 2016, 120, 11381−11394

(11) Field, M. J.; Bash, P. A.; Karplus, M. A Combined Quantum-Mechanical and Molecular Mechanical Potential for Molecular-Dynamics Simulations. *J. Comput. Chem.* **1990**, *11*, 700−733.
(12) Bakowies, D.; Thiel, W. Hybrid Models for Combined Quantum Mechanical and Molecular Mechanical Approaches. *J. Phys. Chem.* **1996**, *100*, 10580−10594.
(13) Mordasini, T. Z.; Thiel, W. Combined Quantum Mechanical and Molecular Mechanical Approaches. *Chimia* **1998**, *52*, 288−291.
(14) Monard, G.; Merz, K. M. Combined Quantum Mechanical/Molecular Mechanical Methodologies Applied to Biomolecular Systems. *Acc. Chem. Res.* **1999**, *32*, 904−911.
(15) Gao, J. L.; Truhlar, D. G. Quantum Mechanical Methods for Enzyme Kinetics. *Annu. Rev. Phys. Chem.* **2002**, *53*, 467−505.
(16) Rosta, E.; Klahn, M.; Warshel, A. Towards Accurate Ab Initio QM/MM Calculations of Free-Energy Profiles of Enzymatic Reactions. *J. Phys. Chem. B* **2006**, *110*, 2934−2941.
(17) Lin, H.; Truhlar, D. QM/MM: What Have We Learned, Where Are We, and Where Do We Go from Here? *Theor. Chem. Acc.* **2007**, *117*, 185−199.
(18) Vidossich, P.; Fiorin, G.; Alfonso-Prieto, M.; Derat, E.; Shaik, S.; Rovira, C. On the Role of Water in Peroxidase Catalysis: A Theoretical Investigation of Hrp Compound I Formation. *J. Phys. Chem. B* **2010**, *114*, 5161−5169.
(19) Senn, H. M.; Thiel, W. QM/MM Methods for Biomolecular Systems. *Angew. Chem., Int. Ed.* **2009**, *48*, 1198−1229.
(20) Carloni, P.; Rothlisberger, U.; Parrinello, M. The Role and Perspective of a Initio Molecular Dynamics in the Study of Biological Systems. *Acc. Chem. Res.* **2002**, *35*, 455−464.
(21) Eurenius, K. P.; Chatfield, D. C.; Brooks, B. R.; Hodoscek, M. Enzyme Mechanisms with Hybrid Quantum and Molecular Mechanical Potentials. I. Theoretical Considerations. *Int. J. Quantum Chem.* **1996**, *60*, 1189−1200.
(22) Senn, H. M.; Thiel, W. QM/MM Studies of Enzymes. *Curr. Opin. Chem. Biol.* **2007**, *11*, 182−187.
(23) Monari, A.; Rivail, J.-L.; Assfeld, X. Theoretical Modeling of Large Molecular Systems. Advances in the Local Self-Consistent Field Method for Mixed Quantum Mechanics/Molecular Mechanics Calculations. *Acc. Chem. Res.* **2013**, *46*, 596−603.
(24) Wang, Y.; Gao, J. Projected Hybrid Orbitals: A General QM/MM Method. *J. Phys. Chem. B* **2015**, *119*, 1213−1224.
(25) Slavicek, P.; Martinez, T. J. Multicentered Valence Electron Effective Potentials: A Solution to the Link Atom Problem for Ground and Excited Electronic States. *J. Chem. Phys.* **2006**, *124*, 084107.
(26) Murphy, R. B.; Philipp, D. M.; Friesner, R. A. A Mixed Quantum Mechanics/Molecular Mechanics (QM/MM) Method for Large Scale Modeling of Chemistry in Protein Environments. *J. Comput. Chem.* **2000**, *21*, 1442−1457.
(27) Zhang, Y.; Lee, T.-S.; Yang, W. A Pseudobond Approach to Combining Quantum Mechanical and Molecular Mechanical Methods. *J. Chem. Phys.* **1999**, *110*, 46−54.
(28) DiLabio, G. A.; Hurley, M. M.; Christiansen, P. A. Simple One-Electron Quantum Capping Potentials for Use in Hybrid QM/MM Studies of Biological Molecules. *J. Chem. Phys.* **2002**, *116*, 9578−9584.
(29) von Lilienfeld, O. A.; Tavernelli, I.; Rothlisberger, U.; Sebastiani, D. Variational Optimization of Effective Atom-Centered Potentials for Molecular Properties. *J. Chem. Phys.* **2005**, *122*, 014113.
(30) Wang, B.; Truhlar, D. G. Combined Quantum Mechanical and Molecular Mechanical Methods for Calculating Potential Energy Surfaces: Tuned and Balanced Redistributed Charge Algorithm. *J. Chem. Theory Comput.* **2010**, *6*, 359−369.
(31) Thellamurege, N. M.; Hirao, H. Effect of Protein Environment within Cytochrome P450cam Evaluated Using a Polarizable-Embedding QM/MM Method. *J. Phys. Chem. B* **2014**, *118*, 2084−2092.
(32) Ponder, J. W.; Wu, C.; Ren, P.; Pande, V. S.; Chodera, J. D.; Schnieders, M. J.; Haque, I.; Mobley, D. L.; Lambrecht, D. S.; DiStasio, R. A., Jr. Current Status of the AMOEBA Polarizable Force Field. *J. Phys. Chem. B* **2010**, *114*, 2549−2564.
(33) Halgren, T. A.; Damm, W. Polarizable Force Fields. *Curr. Opin. Struct. Biol.* **2001**, *11*, 236−242.
(34) Ufimtsev, I. S.; Luehr, N.; Martínez, T. J. Charge Transfer and Polarization in Solvated Proteins from Ab Initio Molecular Dynamics. *J. Phys. Chem. Lett.* **2011**, *2*, 1789−1793.
(35) Nadig, G.; Van Zant, L. C.; Dixon, S. L.; Merz, K. M. Charge-Transfer Interactions in Macromolecular Systems: A New View of the Protein/Water Interface. *J. Am. Chem. Soc.* **1998**, *120*, 5593−5594.
(36) Kulik, H. J.; Luehr, N.; Ufimtsev, I. S.; Martinez, T. J. Ab Initio Quantum Chemistry for Protein Structure. *J. Phys. Chem. B* **2012**, *116*, 12501−12509.
(37) Ufimtsev, I. S.; Martínez, T. J. Quantum Chemistry on Graphical Processing Units. 1. Strategies for Two-Electron Integral Evaluation. *J. Chem. Theory Comput.* **2008**, *4*, 222−231.
(38) Ufimtsev, I. S.; Martínez, T. J. Quantum Chemistry on Graphical Processing Units. 2. Direct Self-Consistent-Field Implementation. *J. Chem. Theory Comput.* **2009**, *5*, 1004−1015.
(39) Ufimtsev, I. S.; Martínez, T. J. Quantum Chemistry on Graphical Processing Units. 3. Analytical Energy Gradients, Geometry Optimization, and First Principles Molecular Dynamics. *J. Chem. Theory Comput.* **2009**, *5*, 2619−2628.
(40) Isborn, C. M.; Luehr, N.; Ufimtsev, I. S.; Martinez, T. J. Excited-State Electronic Structure with Configuration Interaction Singles and Tamm-Dancoff Time-Dependent Density Functional Theory on Graphical Processing Units. *J. Chem. Theory Comput.* **2011**, *7*, 1814−1823.
(41) Ochsenfeld, C.; Kussmann, J.; Lambrecht, D. S. Linear-Scaling Methods in Quantum Chemistry. *Rev. Comput. Chem.* **2007**, *23*, 1.
(42) Eichkorn, K.; Weigend, F.; Treutler, O.; Ahlrichs, R. Auxiliary Basis Sets for Main Row Atoms and Transition Metals and Their Use to Approximate Coulomb Potentials. *Theor. Chem. Acc.* **1997**, *97*, 119−124.
(43) Eichkorn, K.; Treutler, O.; Öhm, H.; Häser, M.; Ahlrichs, R. Auxiliary Basis Sets to Approximate Coulomb Potentials. *Chem. Phys. Lett.* **1995**, *240*, 283−290.
(44) Gaiduk, A. P.; Govoni, M.; Seidel, R.; Skone, J. H.; Winter, B.; Galli, G. Photoelectron Spectra of Aqueous Solutions from First Principles. *J. Am. Chem. Soc.* **2016**, *138*, 6912−6915.
(45) Meier, K.; Thiel, W.; van Gunsteren, W. F. On the Effect of a Variation of the Force Field, Spatial Boundary Condition and Size of the QM Region in QM/MM MD Simulations. *J. Comput. Chem.* **2012**, *33*, 363−378.
(46) Solt, I.; Kulhanek, P.; Simon, I.; Winfield, S.; Payne, M. C.; Csanyi, G.; Fuxreiter, M. Evaluating Boundary Dependent Errors in QM/MM Simulations. *J. Phys. Chem. B* **2009**, *113*, 5728−5735.
(47) Flaig, D.; Beer, M.; Ochsenfeld, C. Convergence of Electronic Structure with the Size of the QM Region: Example of QM/MM NMR Shieldings. *J. Chem. Theory Comput.* **2012**, *8*, 2260−2271.
(48) Hartman, J. D.; Neubauer, T. J.; Caulkins, B. G.; Mueller, L. J.; Beran, G. J. Converging Nuclear Magnetic Shielding Calculations with Respect to Basis and System Size in Protein Systems. *J. Biomol. NMR* **2015**, *62*, 327−340.
(49) Fox, S. J.; Pittock, C.; Fox, T.; Tautermann, C. S.; Malcolm, N.; Skylaris, C. K. Electrostatic Embedding in Large-Scale First Principles Quantum Mechanical Calculations on Biomolecules. *J. Chem. Phys.* **2011**, *135*, 224107.
(50) Liao, R. Z.; Thiel, W. Convergence in the QM-Only and QM/MM Modeling of Enzymatic Reactions: A Case Study for Acetylene Hydratase. *J. Comput. Chem.* **2013**, *34*, 2389−2397.
(51) Sadeghian, K.; Flaig, D.; Blank, I. D.; Schneider, S.; Strasser, R.; Stathis, D.; Winnacker, M.; Carell, T.; Ochsenfeld, C. Ribose-Protonated DNA Base Excision Repair: A Combined Theoretical and Experimental Study. *Angew. Chem., Int. Ed.* **2014**, *53*, 10044−10048.
(52) Isborn, C. M.; Goetz, A. W.; Clark, M. A.; Walker, R. C.; Martinez, T. J. Electronic Absorption Spectra from Mm and Ab Initio QM/MM Molecular Dynamics: Environmental Effects on the Absorption Spectrum of Photoactive Yellow Protein. *J. Chem. Theory Comput.* **2012**, *8*, 5092−5106.

DOI: 10.1021/acs.jpcb.6b07814
J. Phys. Chem. B 2016, 120, 11381−11394

(53) Vanpoucke, D. E.; Oláh, J.; De Proft, F.; Van Speybroeck, V.; Roos, G. Convergence of Atomic Charges with the Size of the Enzymatic Environment. *J. Chem. Inf. Model.* **2015**, *55*, 564−571.
(54) Harris, T. V.; Szilagyi, R. K. Protein Environmental Effects on Iron-Sulfur Clusters: A Set of Rules for Constructing Computational Models for Inner and Outer Coordination Spheres. *J. Comput. Chem.* **2016**, *37*, 1681−1696.
(55) Sumowski, C. V.; Ochsenfeld, C. A Convergence Study of QM/MM Isomerization Energies with the Selected Size of the QM Region for Peptidic Systems†. *J. Phys. Chem. A* **2009**, *113*, 11734−11741.
(56) Sumner, S.; Söderhjelm, P.; Ryde, U. Effect of Geometry Optimizations on QM-Cluster and QM/MM Studies of Reaction Energies in Proteins. *J. Chem. Theory Comput.* **2013**, *9*, 4205−4214.
(57) Hu, L.; Söderhjelm, P.; Ryde, U. Accurate Reaction Energies in Proteins Obtained by Combining QM/MM and Large QM Calculations. *J. Chem. Theory Comput.* **2013**, *9*, 640−649.
(58) Hu, L.; Söderhjelm, P.; Ryde, U. On the Convergence of QM/MM Energies. *J. Chem. Theory Comput.* **2011**, *7*, 761−777.
(59) Hu, L.; Eliasson, J.; Heimdal, J.; Ryde, U. Do Quantum Mechanical Energies Calculated for Small Models of Protein-Active Sites Converge?†. *J. Phys. Chem. A* **2009**, *113*, 11793−11800.
(60) Rudberg, E.; Rubensson, E. H.; Salek, P. Kohn-Sham Density Functional Theory Electronic Structure Calculations with Linearly Scaling Computational Time and Memory Usage. *J. Chem. Theory Comput.* **2011**, *7*, 340−350.
(61) Challacombe, M.; Schwegler, E. Linear Scaling Computation of the Fock Matrix. *J. Chem. Phys.* **1997**, *106*, 5526−5536.
(62) Skylaris, C.-K.; Haynes, P. D.; Mostofi, A. A.; Payne, M. C. Introducing ONETEP: Linear Scaling Density Functional Simulations on Parallel Computers. *J. Chem. Phys.* **2005**, *122*, 084119.
(63) Bowler, D. R.; Miyazaki, T. O(N) Methods in Electronic Structure Calculations. *Rep. Prog. Phys.* **2012**, *75*, 036503.
(64) VandeVondele, J.; Borštnik, U.; Hutter, J. Linear Scaling Self-Consistent Field Calculations with Millions of Atoms in the Condensed Phase. *J. Chem. Theory Comput.* **2012**, *8*, 3565−3573.
(65) Scuseria, G. E. Linear Scaling Density Functional Calculations with Gaussian Orbitals. *J. Phys. Chem. A* **1999**, *103*, 4782−4790.
(66) Guidon, M.; Hutter, J.; VandeVondele, J. Robust Periodic Hartree-Fock Exchange for Large-Scale Simulations Using Gaussian Basis Sets. *J. Chem. Theory Comput.* **2009**, *5*, 3010−3021.
(67) Mori-Sánchez, P.; Cohen, A. J.; Yang, W. Many-Electron Self-Interaction Error in Approximate Density Functionals. *J. Chem. Phys.* **2006**, *125*, 201102.
(68) Ruzsinszky, A.; Perdew, J. P.; Csonka, G. I.; Vydrov, O. A.; Scuseria, G. E. Density Functionals That Are One- and Two- Are Not Always Many-Electron Self-Interaction-Free, as Shown for H2+, He2+, LiH+, and Ne2+. *J. Chem. Phys.* **2007**, *126*, 104102.
(69) Haunschild, R.; Henderson, T. M.; Jiménez-Hoyos, C. A.; Scuseria, G. E. Many-Electron Self-Interaction and Spin Polarization Errors in Local Hybrid Density Functionals. *J. Chem. Phys.* **2010**, *133*, 134116.
(70) Cohen, A. J.; Mori-Sánchez, P.; Yang, W. Insights into Current Limitations of Density Functional Theory. *Science* **2008**, *321*, 792−794.
(71) Schmidt, T.; Kümmel, S. One- and Many-Electron Self-Interaction Error in Local and Global Hybrid Functionals. *Phys. Rev. B: Condens. Matter Mater. Phys.* **2016**, *93*, 165120.
(72) Ruzsinszky, A.; Perdew, J. P.; Csonka, G. I.; Vydrov, O. A.; Scuseria, G. E. Spurious Fractional Charge on Dissociated Atoms: Pervasive and Resilient Self-Interaction Error of Common Density Functionals. *J. Chem. Phys.* **2006**, *125*, 194112.
(73) Dutoi, A. D.; Head-Gordon, M. Self-Interaction Error of Local Density Functionals for Alkali−Halide Dissociation. *Chem. Phys. Lett.* **2006**, *422*, 230−233.
(74) Bally, T.; Sastry, G. N. Incorrect Dissociation Behavior of Radical Ions in Density Functional Calculations. *J. Phys. Chem. A* **1997**, *101*, 7923−7925.
(75) Zhang, Y.; Yang, W. A Challenge for Density Functionals: Self-Interaction Error Increases for Systems with a Noninteger Number of Electrons. *J. Chem. Phys.* **1998**, *109*, 2604−2608.
(76) Johnson, B. G.; Gonzales, C. A.; Gill, P. M. W.; Pople, J. A. A Density Functional Study of the Simplest Hydrogen Abstraction Reaction. Effect of Self-Interaction Correction. *Chem. Phys. Lett.* **1994**, *221*, 100−108.
(77) Axelrod, J.; Tomchick, R. Enzymatic O-Methylation of Epinephrine and Other Catechols. *J. Biol. Chem.* **1958**, *233*, 702−705.
(78) Lotta, T.; Vidgren, J.; Tilgmann, C.; Ulmanen, I.; Melen, K.; Julkunen, I.; Taskinen, J. Kinetics of Human Soluble and Membrane-Bound Catechol O-Methyltransferase: A Revised Mechanism and Description of the Thermolabile Variant of the Enzyme. *Biochemistry* **1995**, *34*, 4202−4210.
(79) Cheng, X.; Kumar, S.; Posfai, J.; Pflugrath, J. W.; Roberts, R. J. Crystal Structure of the Hhal DNA Methyltransferase Complexed with S-Adenosyl-L-Methionine. *Cell* **1993**, *74*, 299−307.
(80) Labahn, J.; Granzin, J.; Schluckebier, G.; Robinson, D. P.; Jack, W. E.; Schildkraut, I.; Saenger, W. Three-Dimensional Structure of the Adenine-Specific DNA Methyltransferase M.Taq I in Complex with the Cofactor S-Adenosylmethionine. *Proc. Natl. Acad. Sci. U. S. A.* **1994**, *91*, 10957−10961.
(81) Lau, E. Y.; Bruice, T. C. Importance of Correlated Motions in Forming Highly Reactive near Attack Conformations in Catechol O-Methyltransferase. *J. Am. Chem. Soc.* **1998**, *120*, 12387−12394.
(82) Zhang, J.; Kulik, H. J.; Martinez, T. J.; Klinman, J. P. Mediation of Donor−Acceptor Distance in an Enzymatic Methyl Transfer Reaction. *Proc. Natl. Acad. Sci. U. S. A.* **2015**, *112*, 7954−7959.
(83) Roca, M.; Andrés, J.; Moliner, V.; Tuñón, I.; Bertrán, J. On the Nature of the Transition State in Catechol O-Methyltransferase. A Complementary Study Based on Molecular Dynamics and Potential Energy Surface Explorations. *J. Am. Chem. Soc.* **2005**, *127*, 10648−10655.
(84) Kanaan, N.; Ruiz Pernia, J. J.; Williams, I. H. QM/MM Simulations for Methyl Transfer in Solution and Catalysed by COMT: Ensemble-Averaging of Kinetic Isotope Effects. *Chem. Commun.* **2008**, 6114−6116.
(85) Axelrod, J. J. Methylation Reactions in the Formation and Metabolism of Catecholamines and Other Biogenic Amines. *Pharmacol. Rev.* **1966**, *18*, 95−113.
(86) Kuhn, B.; Kollman, P. A. QM−FE and Molecular Dynamics Calculations on Catechol O-Methyltransferase: Free Energy of Activation in the Enzyme and in Aqueous Solution and Regioselectivity of the Enzyme-Catalyzed Reaction. *J. Am. Chem. Soc.* **2000**, *122*, 2586−2596.
(87) Tsao, D.; Liu, S.; Dokholyan, N. V. Regioselectivity of Catechol O-Methyltransferase Confers Enhancement of Catalytic Activity. *Chem. Phys. Lett.* **2011**, *506*, 135−138.
(88) Lameira, J.; Bora, R. P.; Chu, Z. T.; Warshel, A. Methyltransferases Do Not Work by Compression, Cratic, or Desolvation Effects, but by Electrostatic Preorganization. *Proteins: Struct., Funct., Genet.* **2015**, *83*, 318−330.
(89) Rutherford, K.; Le Trong, I.; Stenkamp, R. E.; Parson, W. W. Crystal Structures of Human 108V and 108M Catechol O-Methyltransferase. *J. Mol. Biol.* **2008**, *380*, 120−130.
(90) Anandakrishnan, R.; Aguilar, B.; Onufriev, A. V. H++ 3.0: Automating pK Prediction and the Preparation of Biomolecular Structures for Atomistic Molecular Modeling and Simulations. *Nucleic Acids Res.* **2012**, *40*, W537−W541.
(91) Gordon, J. C.; Myers, J. B.; Folta, T.; Shoja, V.; Heath, L. S.; Onufriev, A. H++: A Server for Estimating pKas and Adding Missing Hydrogens to Macromolecules. *Nucleic Acids Res.* **2005**, *33*, W368−W371.
(92) Myers, J.; Grothaus, G.; Narayanan, S.; Onufriev, A. A Simple Clustering Algorithm Can Be Accurate Enough for Use in Calculations of pKs in Macromolecules. *Proteins: Struct., Funct., Genet.* **2006**, *63*, 928−938.

DOI: 10.1021/acs.jpcb.6b07814
J. Phys. Chem. B 2016, 120, 11381−11394

(93) Case, D. A.; Darden, T. A.; Cheatham, T. E.; Simmerling, C. L.; Wang, J.; Duke, R. E.; Luo, R.; Walker, R. C.; Zhang, W.; Merz, K. M., et al. *Amber 12*; University of California: San Francisco, CA, 2012.
(94) Henkelman, G.; Uberuaga, B. P.; Jonsson, H. A Climbing Image Nudged Elastic Band Method for Finding Saddle Points and Minimum Energy Paths. *J. Chem. Phys.* **2000**, *113*, 9901−9904.
(95) Petachem. http://www.petachem.com. (accessed July 1, 2016).
(96) Rohrdanz, M. A.; Martins, K. M.; Herbert, J. M. A Long-Range-Corrected Density Functional That Performs Well for Both Ground-State Properties and Time-Dependent Density Functional Theory Excitation Energies, Including Charge-Transfer Excited States. *J. Chem. Phys.* **2009**, *130*, 054112.
(97) Ditchfield, R.; Hehre, W. J.; Pople, J. A. Self-Consistent Molecular Orbital Methods. IX. An Extended Gaussian-Type Basis for Molecular Orbital Studies of Organic Molecules. *J. Chem. Phys.* **1971**, *54*, 724.
(98) *The PyMOL Molecular Graphics System*, version 1.7.4.3; Schrodinger, LLC, 2010.
(99) Guerra, C. F.; Handgraaf, J. W.; Baerends, E. J.; Bickelhaupt, F. M. Voronoi Deformation Density (VDD) Charges: Assessment of the Mulliken, Bader, Hirshfeld, Weinhold, and VDD Methods for Charge Analysis. *J. Comput. Chem.* **2004**, *25*, 189−210.
(100) Tozer, D. J.; De Proft, F. Computation of the Hardness and the Problem of Negative Electron Affinities in Density Functional Theory. *J. Phys. Chem. A* **2005**, *109*, 8923−8929.
(101) Teale, A. M.; De Proft, F.; Tozer, D. J. Orbital Energies and Negative Electron Affinities from Density Functional Theory: Insight from the Integer Discontinuity. *J. Chem. Phys.* **2008**, *129*, 044110.
(102) Peach, M. J. G.; Teale, A. M.; Helgaker, T.; Tozer, D. J. Fractional Electron Loss in Approximate DFT and Hartree−Fock Theory. *J. Chem. Theory Comput.* **2015**, *11*, 5262−5268.
(103) Rudberg, E. Difficulties in Applying Pure Kohn−Sham Density Functional Theory Electronic Structure Methods to Protein Molecules. *J. Phys.: Condens. Matter* **2012**, *24*, 072202.
(104) Lever, G.; Cole, D. J.; Hine, N. D. M.; Haynes, P. D.; Payne, M. C. Electrostatic Considerations Affecting the Calculated HOMO-LUMO Gap in Protein Molecules. *J. Phys.: Condens. Matter* **2013**, *25*, 152101.
(105) Isborn, C. M.; Mar, B. D.; Curchod, B. F. E.; Tavernelli, I.; Martinez, T. J. The Charge Transfer Problem in Density Functional Theory Calculations of Aqueously Solvated Molecules. *J. Phys. Chem. B* **2013**, *117*, 12189−12201.
(106) Lee, C.; Yang, W.; Parr, R. G. Development of the Colle-Salvetti Correlation-Energy Formula into a Functional of the Electron Density. *Phys. Rev. B: Condens. Matter Mater. Phys.* **1988**, *37*, 785−789.
(107) Becke, A. D. Density-Functional Thermochemistry. III. The Role of Exact Exchange. *J. Chem. Phys.* **1993**, *98*, 5648−5652.
(108) Stephens, P. J.; Devlin, F. J.; Chabalowski, C. F.; Frisch, M. J. Ab Initio Calculation of Vibrational Absorption and Circular Dichroism Spectra Using Density Functional Force Fields. *J. Phys. Chem.* **1994**, *98*, 11623−11627.
(109) Bonifácio, M. J.; Archer, M.; Rodrigues, M. L.; Matias, P. M.; Learmonth, D. A.; Carrondo, M. A.; Soares-da-Silva, P. c. Kinetics and Crystal Structure of Catechol-O-Methyltransferase Complex with Co-Substrate and a Novel Inhibitor with Potential Therapeutic Application. *Mol. Pharmacol.* **2002**, *62*, 795−805.
(110) Vidgren, J.; Svensson, L. A.; Liljas, A. Crystal Structure of Catechol O-Methyltransferase. *Nature* **1994**, *368*, 354−358.
(111) Palma, P. N.; Rodrigues, M. L.; Archer, M.; Bonifácio, M. J.; Loureiro, A. I.; Learmonth, D. A.; Carrondo, M. A.; Soares-da-Silva, P. Comparative Study of Ortho- and Meta-Nitrated Inhibitors of Catechol-O-Methyltransferase: Interactions with the Active Site and Regioselectivity of O-Methylation. *Mol. Pharmacol.* **2006**, *70*, 143−153.
(112) Tsuji, E.; Okazaki, K.; Takeda, K. Crystal Structures of Rat Catechol-O-Methyltransferase Complexed with Coumarine-Based Inhibitor. *Biochem. Biophys. Res. Commun.* **2009**, *378*, 494−497.
(113) Ellermann, M.; Lerner, C.; Burgy, G.; Ehler, A.; Bissantz, C.; Jakob-Roetne, R.; Paulini, R.; Allemann, O.; Tissot, H.; Grunstein, D.; et al. Catechol-O-Methyltransferase in Complex with Substituted 3′-Deoxyribose Bisubstrate Inhibitors. *Acta Crystallogr., Sect. D: Biol. Crystallogr.* **2012**, *68*, 253−260.
(114) Harrison, S. T.; Poslusney, M. S.; Mulhearn, J. J.; Zhao, Z.; Kett, N. R.; Schubert, J. W.; Melamed, J. Y.; Allison, T. J.; Patel, S. B.; Sanders, J. M.; et al. Synthesis and Evaluation of Heterocyclic Catechol Mimics as Inhibitors of Catechol-O-Methyltransferase (COMT). *ACS Med. Chem. Lett.* **2015**, *6*, 318−323.
(115) Ruggiero, G. D.; Williams, I. H.; Roca, M.; Moliner, V.; Tunon, I. QM/MM Determination of Kinetic Isotope Effects for COMT-Catalyzed Methyl Transfer Does Not Support Compression Hypothesis. *J. Am. Chem. Soc.* **2004**, *126*, 8634−8635.
(116) Schultz, E.; Nissinen, E. Inhibition of Rat Liver and Duodenum Soluble Catechol-O-Methyltransferase by a Tight-Binding Inhibitor or-462. *Biochem. Pharmacol.* **1989**, *38*, 3953−3956.
(117) Rod, T. H.; Rydberg, P.; Ryde, U. Implicit Versus Explicit Solvent in Free Energy Calculations of Enzyme Catalysis: Methyl Transfer Catalyzed by Catechol O-Methyltransferase. *J. Chem. Phys.* **2006**, *124*, 174503.
(118) Sparta, M.; Alexandrova, A. N. How Metal Substitution Affects the Enzymatic Activity of Catechol-O-Methyltransferase. *PLoS One* **2012**, *7*, e47172.
(119) Mihel, I.; Knipe, J. O.; Coward, J. K.; Schowen, R. L. Alpha.-Deuterium Isotope Effects and Transition-State Structure in an Intramolecular Model System for Methyl-Transfer Enzymes. *J. Am. Chem. Soc.* **1979**, *101*, 4349−4351.
(120) Rodgers, J.; Femec, D. A.; Schowen, R. L. Isotopic Mapping of Transition-State Structural Features Associated with Enzymic Catalysis of Methyl Transfer. *J. Am. Chem. Soc.* **1982**, *104*, 3263−3268.
(121) Wong, K. F.; Watney, J. B.; Hammes-Schiffer, S. Analysis of Electrostatics and Correlated Motions for Hydride Transfer in Dihydrofolate Reductase. *J. Phys. Chem. B* **2004**, *108*, 12231−12241.
(122) Bash, P. A.; Field, M. J.; Davenport, R. C.; Petsko, G. A.; Ringe, D.; Karplus, M. Computer Simulation and Analysis of the Reaction Pathway of Triosephosphate Isomerase. *Biochemistry* **1991**, *30*, 5826−5832.

DOI: 10.1021/acs.jpcb.6b07814
J. Phys. Chem. B 2016, 120, 11381−11394